GNSS-Based GNC System Design, Development and Analysis of a Large-Scale Autonomous Delta-Wing CanSat Model for Explorational Purposes

Peeramed Chodkaveekityada*, Bhavat Ngamdeevilaisak†, Chayanin Uthanpathumros†, Kittiphop Vichitkijja†, Kolawat Dendeevanich†, Nutthamet Sriprachayanan†, Vivatsathorn Thitasirivit† and Phachara Phumiprathet†

*Faculty of Engineering, King Mongkut's Institute of Technology Ladkrabang, Bangkok, Thailand
†ALPACA Team, Assumption College, Bangkok, Thailand

***Abstract*—A CanSat is a miniaturized simulation model of a real satellite, enclosed within a cylindrical structure, operating under atmospheric conditions, mainly used for various purposes, one of which includes a deployable delta-wing aircraft payload enclosed in a CanSat container, consisting of major subsystems including mechanical, communication and electronic subsystem. The CanSat is then launched into an atmosphere at the altitude of 700 meters by a rocket or deployed from an unmanned aerial vehicle. The missions of study are to measure data from telemetry sensors and to implement the GNC method for wayfinding by interpolating the marked coordinates for smooth path and extrapolating for next point prediction and by implementing a convex hull algorithm to create an exploration route within a study area. In comparison to a quadcopter or similar alternatives, a delta wing has significantly lower energy consumption as the wings are used as main lift for this type of subsonic aircraft and has more compactness, hence able to fit in rocket and deploy at higher altitude. The model is a scaled-up prototype based on the requirements of CanSat Competition 2020 which surpassed Critical Design Review round. The delta wing is deployed from a CanSat container and provoke a thrust for an airfoil to generate a lift and forward speed; the direction is controlled by adjusting aerodynamic properties of the delta wing. The GNC system implemented in a delta wing is widely applied in the exploratory field of study including area survey and observation for analytical purposes. This paper will elaborate the development, design, analysis, comparison and applications of the navigation system and the delta-wing.**

***Index Terms*—CanSat, Delta Wing, Exploration, Guidance Navigation and Control.**

I. Introduction

IT is well known that exploration is important to atmospheric, space and exoplanetary researches and studies. Although rovers and ground vehicles are mainly used to explore the topography, underground chemical compounds and atmospheric conditions, there are several limitations encountering extreme landscapes. Aerial surveys, including Unmanned Aerial Vehicle (UAV) and satellites, are the solutions to the problem due to its higher degree of freedom (DOF), including roll, pitch and yaw. Both unmanned quadcopter and helicopter are mostly used for exploring small-scale study area at relatively low altitude in a certain atmosphere. On the other hand, wing-based aircraft are more energy-efficient and can be deployed at significantly higher altitude for more study area coverage, hence higher data samples and lower number of iterations to be made. Besides, the wing can be made compact by either folding or sliding mechanism and can be fit as a payload for rocket deployment.

One of the major parts of an operation is guidance, navigation and control (GNC) system which controls the path of mission, stabilizes such wing-based aircraft and restrain the direction of it by utilizing all mechanical components, under controls of software, to adjust the value of DOF using aerodynamic properties. Being pervasive in autonomous vehicle control in agriculture, transportation, communication, etc. fields, the Global Navigation Satellite System (GNSS) is used as a substructure of a GNC system; likewise, a large-scale aircraft uses it for its guidance system. Moreover, despite susceptibility to false location determination due to obstacles or other factors, its precision and accuracy at high altitude [16], low refresh rate and short delay interval is outstanding comparing to ground-based referencing methods.

For the GNC system to cooperate with adjustment of aircraft's (delta wing's) aerodynamic properties, an algorithm for determining preferable paths and adjusting flight direction is contrived. As there are many algorithms to determine an enclosed loop path, such as orthogonal convex hull, gift wrapping, etc. (see [2], [6], [12], [14], [21]), a modified Graham's algorithm stated in [24] is used for determining path consisting of a set of GNSS coordinates. Also, transferring between the path of selected coordinates is based on least azimuth angle between two trans-coordinates. A propulsion system is, in addition, used for providing thrust, adjusting forward speed to a desired value. Being widespread in mechanical electronics, aviation, unmanned aircraft, etc. fields, a proportional-integral-derivative (PID) algorithm is implemented in GNC system of our delta wing design (see [9], [17], [18]).

This study aims to create, test, analyze and compare a delta wing CanSat model at actual performance with other prototypes and theoretical simulation and to deploy the CanSat

model in a designated mission. Accordingly, that of CanSat is to be deployed with a rocket and travel in a path consisting of multiple coordinates.

As of CanSat Competition 2020 event, organized by American Astronautical Society (AAS) in United States of America, ALPACA team has surpassed the Preliminary Design Review round and Critical Design Review round. The mission of the competition was to create a similar CanSat model, fit in a 125.00-millimeter-diameter with 300.00-millimeter-height cylinder, which deploys a delta wing glider and glides in a circular pattern. Thus, a modified prototype is created at higher scale with an additional propulsion system as it has less constraints and limitations than in the competition.

There are a number of applications to the model; exploration is the most relevant part which is based on surveying and obtaining atmospheric and topographic data of a study area to use the data for further analysis, one of which is calculating the suitability score of habitability or agriculture [26], [27].

II. System Overview

A. Concept of Operations

The CanSat, consisting of a delta wing and a container is firstly launched into an atmosphere at the altitude ranging from 750 meters to 2000 meters via solid-propellant rocket. As it reaches the apogee, the CanSat is, then, deployed and descends with a parachute until it reaches 30% of the apogee altitude above ground level which is the point where the delta wing is separated from the container with specific releasing mechanism.

After the separation stage, the container continues to descend to the ground; conversely, the delta wing deploys its folded wings on two sides and provoke the initial thrust to gain speed of 25.0 $\mathrm{m \cdot s^{-1}}$. Henceforth, the delta wing glides in a specified coordinates path and collect environmental and inertial sensors data. The data is wirelessly sent to a dedicated ground control station; it is, later, displayed and saved on a ground station portable computer.

The measured atmospheric data can be useful for further analysis, for example, calculation of suitability of living in a certain area. On the other hand, motion and inertial data are analyzed to compare the actual and simulated theoretical performance. Accordingly, the suitability score based on beta probability density function is derived for this type of analysis [26], [27].

B. CanSat Science Payload Layout

The science payload which is a delta wing model layout and transparent view are shown in Fig. 1 and 2.

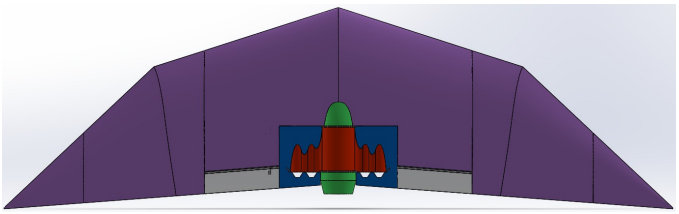

Fig. 1. A boundary representation (BRep) 3D Model of a delta wing science payload.

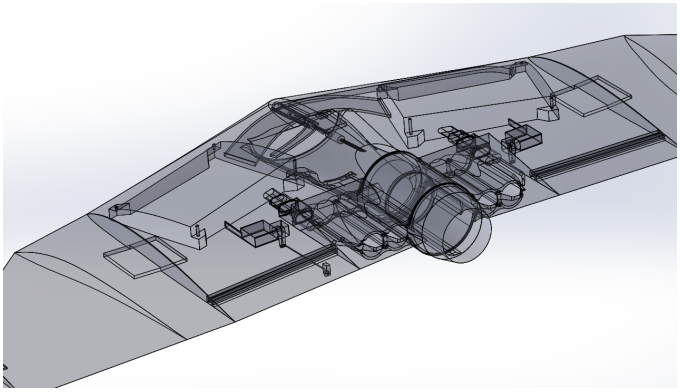

Fig. 2. A transparent view of a delta wing science payload.

III. Electronic and Power Subsystem

Electronic components in the CanSat is classified into five sections by their functionalities:

1) Power Subsystem;
2) Sensor Subsystem;
3) Communication and Data Storage Subsystem;
4) Central Processor Subsystem;
5) Propulsion Controlling Subsystem.

However, in this context, they are categorized into operational elements and power managing elements.

A. Electronics and Sensors

The list of electronic components and sensors excluding passive components are shown in Table I. Not needing a specific module to fulfill the requirements for some measurements, customized specific circuitry are designed on prerequisite. The sensor chips are extracted from modules to be implemented on main printed circuit boards (PCB) to reduce the space required.

B. Circuitry Design

The design concept is to reduce spacing between each component as much as possible without escalating interference by inducing environment signal. Being preferable for complicated layout, two double-sided plated-through-hole PCB with thickness of 1.0 mm are selected as it can significantly reduce the weight of circuit without sacrificing overall stiffness.

C. Sensors Placements

Sensors functions and constraints are used to restrict the placement of sensors in order to prevent it from misconceiving, for instance, temperature-sensitive components are positioned as far from components which tend to heat up as possible. For example, the placement of BME280 (temperature sensor) is required to be distant from voltage converter module.

TABLE I
SENSORS AND HARDWARE DESCRIPTION

Name	Description
Teensy 4.0	Main processor unit for handling calculations and numerical data
BME280	Temperature, humidity and air pressure sensor
BNO055	Inertial measurement unit (IMU): accelerometer, gyroscope, and magnetometer
ATGM336H	Global Navigation Satellite System (GNSS) using Global Positioning System (GPS) Protocol Sensor Module
PMS7003	Air particulate Sensor
MPXV7002	Differential Pressure Sensor
SPI microSD Card Reader	microSD Card Reader module connected to Teensy
Zigbee Xbee 3 Pro	2.4 GHz Radio Communication Module
IRFZ44N	MOSFET used as a switch for Nichrome wire
LEDs and Buzzer	Audio beacon and status indicator
Raspberry Pi Zero W	Camera controller running Raspberry Pi OS

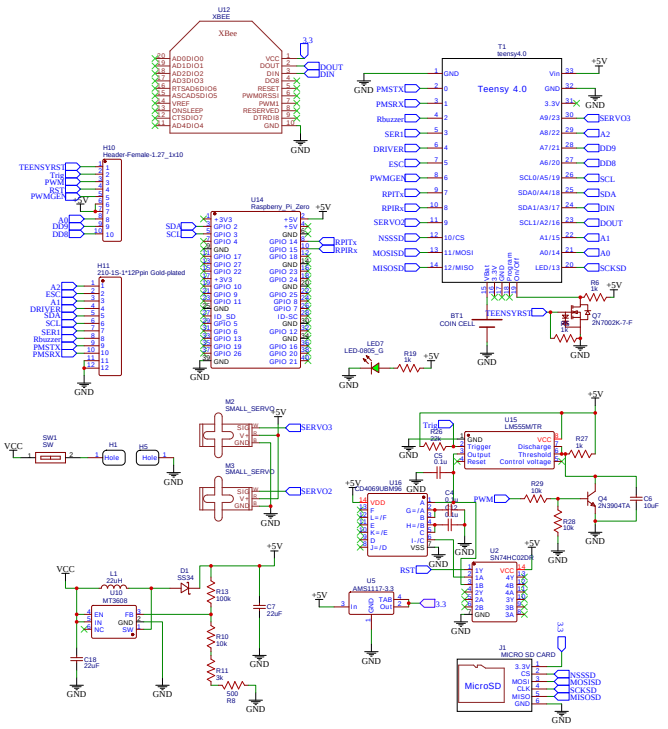

Fig. 3. An electronic subsystems design schematic.

D. Electrical Power Management

Generating the most heat, the power management system is located on the topmost layer as the airflow aids in cooling the components. Each component requires different voltage level ranging from 3.3 V and 5.0 V for most sensors and components and 12.6 V for Electric Ducted Fan (EDF). Two battery systems are configured as follows.

1) One Lithium-ion (Li-ion) battery with 3150 mAh capacity is utilized for supplying controlling subsystems: sensor subsystems and relevant components. The system can theoretically operate up to 4 hours 35 minutes according to the calculation in Table II.
2) Three Li-ion batteries with a total capacity of 2000 mAh supplies the EDF motor. The operation time is up to 1 minute 48 seconds as indicated in Table III.

TABLE II
PAYLOAD CONTROLLING SUBSYSTEMS POWER CONSUMPTION

Hardware (Controlling)	Power (mW)	Duty Cycle	Hardware (EDF)	Power (mW)	Duty Cycle
Teensy 4.0	330.00	100	Raspberry Pi Zero W	1300.00	100
PMS7003	500.00	100	BME280	3.30	100
BNO055	0.66	100	ATGM336H	82.50	100
microSD SPI	16.50	70	Xbee 3 Pro	445.50	50
LEDs and others	200.50	100	**Total**	**2471.26**	**-**

TABLE III
EDF MOTOR SUBSYSTEMS POWER CONSUMPTION

Hardware (EDF)	Power (mW)	Duty Cycle
Heating Coil	22.20	1
EDF	246.45	100
Total	**246.58**	**-**

This configuration which separates the power systems can reduce the power surge when the EDF starts as measured by an oscilloscope in Fig. 4. In case of fully drained EDF batteries, the control system continues working on a dependency of another battery system.

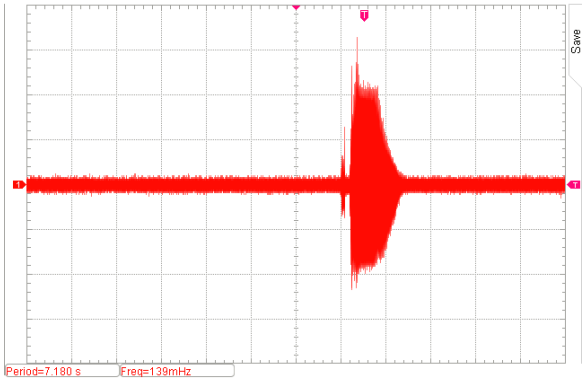

Fig. 4. Graph showing EDF motor electric current surge on start.

IV. DESCENT CONTROL

The descent control is the main mechanical part controlled by flight controlling software which is implemented so that both subsystems can cooperate. It has three parts of operations: A propulsion system for generating an initial thrust, an airfoil and a wing for gliding stage and a parachute for

final declination. Each part performs different operations and purposes. The mission to glide from coordinate to coordinate is mainly based on a wing and a required propulsion system working coordinately to bring forth the functionality into an action.

A. Wing Shape and Airfoil Selection

The delta wing flight and declination are based on gliding with initial thrust to generate a lift and forward speed. The selected airfoil has similar characteristics to airfoil of gliders in terms of shape, lift-to-drag ratio and low-Reynolds-number characteristic.

The selected airfoil shape is model Selig S7055 (10.5%) Flat-Bottomed. It has max thickness of 10.5% at 31.8% chord and max camber of 3.3% at 38.6% chord. Although a flat-bottomed airfoil is design to reduce the drag induced by separation bubble during transition, it has an associated performance penalty and noticeable performance loss at low lift as the geometry of the airfoil is constrained, comparing to non-flat-bottomed airfoil, such as SD7037, WASP, E387 and K3311. The S7055 airfoil geometry plot is shown in Fig. 5. at 100% thickness.

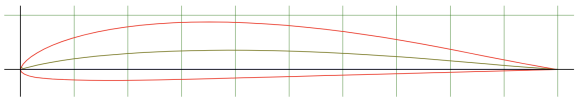

Fig. 5. Selig S7055 (10.5%) Flat-Bottomed airfoil geometry plot with camber line at 100% thickness.

Nevertheless, it has more lift than S3021 or E205. As the delta wing is required to effectuate the propulsion system and the electronic subsystem, flat-bottomed airfoil, in which is more geometrically ideal to fit, is considered. XFLR5 airfoil analysis and simulation software is used to create an ideal shape for a delta wing from multiple constraints and variables, for instance, dihedral of the wings. Using Reynolds number (Re) from 1000 to 1 500 000 with increments of 5000, Ncrit value of 9.00 and ranges from -10.0 degrees to 20.0 degrees angle of attack (α) with increments of 0.1 degrees, the lift coefficient (c_L) to drag coefficient (c_D) graph is generated as shown in Fig. 6.

Being cut out for implementing the propulsion system, printed circuit boards, wires and controllable mechanical components, some portions of the airfoil are unusable for generating a lift, so the characteristics of the delta wing are changed and not aerodynamically ideal when simulated in XFLR5. The performance of an airfoil entails theoretical and actual lift-to-drag ratio, lift force, induced drag, vortex of the delta wing. The simulation and measurement of the delta wing includes a variety of components besides the embedded airfoil. The theoretical performance of the airfoil is simulated with a high resolution to-scale mesh 3D model. Moreover, the actual performance is measured by means of wind tunnel testing.

The characteristics of S7055 airfoil depend on shape of wings, for instance, different taper ratio of two wings can have different aerodynamic characteristics and advantages in terms of induced drag, lift force and wing area. The delta wing is

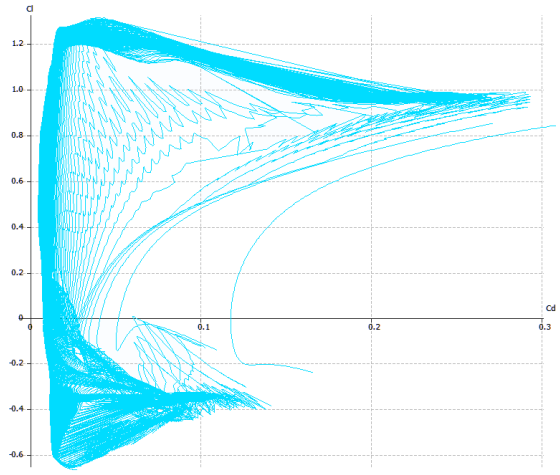

Fig. 6. Multi-threaded batch analysis of c_L to c_D graph generated by XFLR5 using XFoil Direct Analysis tool.

chosen due to its larger wing area and stability comparing to other types of wings without sacrificing the advantages of the wings. The delta wing is enclosed in the compartment area of the CanSat container, folded to fit inside 390.00-millimeter-diameter with 280.00-millimeter-height cylindrical partition. Because of its large circuit boards, batteries and propulsion system, a delta wing is an ideal shape for implementing that of systems to fit in with less performance loss due to the reduction of an airfoil area. Due to the delta wing aerodynamic, it needs relatively high angle of attack and forward speed, comparing to other types of wings to maintain lift. Comparing between 10.0, 15.0, 20.0 and 25.0 $\mathrm{m \cdot s^{-1}}$, it is shown in Fig. 7. that in the same ranges of angle of attack, each lift-to-drag ratio (c_L/c_D) is directly proportional to the forward speed, for instance, 25.0 $\mathrm{m \cdot s^{-1}}$ has the highest c_L/c_D among simulated flight speed.

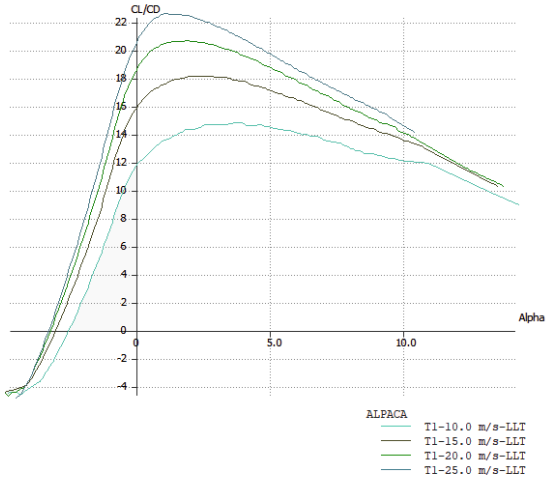

Fig. 7. Graph showing comparison of lift-to-drag coefficient and angle of attack with forward speed between 10.0, 15.0, 20.0 and 25.0 $\mathrm{m \cdot s^{-1}}$.

Furthermore, the delta wing is designed for high-speed usage and has unenviable characteristics at low speed flight.

As a result of high angle of attack, a vortex is generated from each leading edge of the wing on the upper surface and thus increased drag and stability. In consequence, an effective and well-designed propulsion system is needed to maintain the lift at low speed and high-angle-of-attack flight. For controlling the angle of attack and adjusting roll and pitch angle of an aircraft, elevons are located on two sides and utilized simultaneously and accordingly to perform a change in or stabilization of the heading direction.

B. Propulsion System

Generating a lift force from a wing, it needs an initial thrust and continuous thrust to maintain the gradual descending stages of the aircraft. On account of its small scale, a propulsion system based on fuel or a combustion engine could not be used in the delta wing. An electric ducted fan (EDF Thruster) is, instead, used as it has comparatively less size than other electric-motor-based system, for example, two-blade propellers. In addition, an EDF has significantly less rotational moment than the latter with equivalent power usage, hence no counterrotation needed. The selected EDF has 4.0 N of thrust for accelerating the delta wing to desired forward speed, has 40.0 mm diameter with eight blades and uses 330.0 W at 11.1 V using Li-ion battery. It is controlled by an electronic speed controller (ESC) locating inside the intake vent with sufficient heat dissipation from high-speed intake air and being able to withstand 65-A electric current.

C. Parachute Rescue System Design

Parachute rescue system is employed during the descending stage for both delta wing and container. After ejected from the rocket or any other means of ejection, the container's parachutes are instantly deployed, resulted in declining to constant descent velocity. Ringsail design is used for the rescue system, introduced in many manned spacecraft recovery applications including Apollo landing system, due to its characteristics are more stability and evenly inflated than conventional flat circular parachutes which has very poor opening characteristic as elaborated in [23], [13]. Consisting of rings in the canopy area, the pendulum swing and risk of being stuck inside deployment chamber is also reduced and withal instigate more opening stability and rapid with soft billowing flow and constant rate according to [10]. The nominal cloth area S_0, canopy nominal diameter D_0 and suspension lines' length l_e using equations:

$$S_0 = \frac{c_D S}{c_{D,0}} \tag{1}$$

$$D_0 = \sqrt{\frac{4S_0}{\pi}} \tag{2}$$

$$l_e = 1.15 D_0 \tag{3}$$

while

- Drag coefficient $c_{D,0} = 0.850$;
- Nominal cloth area $S_0 = 0.452$ m^2;
- Nominal diameter $D_0 = 0.625$ m;
- Suspension lines' length $l_e = 0.718$ m;
- Number of rings $N_r = 5$;
- Number of suspension lines $N_e = 12$.

As a result, the calculated velocity is 12 m $\cdot$ s^{-1} and different opening time and distance are noticed comparing to flat circular parachute. The nominal drag coefficient c_D of flat circular parachute is 1.36 which is relatively higher than the ringsail parachute, hence higher surface area needed.

V. Mechanical Subsystem

A. Material Selection and Structures

Considering structural strength and characteristic of an aircraft, low-weight-but-high-rigidity material with accurate model creation is essential for airfoil design in real world usages. Most small-scale delta wing uses polystyrene as a main structure due to its particularly optimal weight to strength ratio. Alternatively, ribbed wood structure covered with plastic sheet is, also, used in this field. Plastic model printing based on designed 3D model is the best choice for creating a unique design, being customizable. Fused deposition modeling (FDM) 3D-printing technique is used for printing complex assembly designs, one of which is CanSat (and also other related designs, e.g. CubeSat). The infill density of printed parts is also variable based on the weight needed; moreover, the time and cost efficiency and dimensional accuracy is also considered for fabricating designated dimensions.

B. 3D-Printing Material Selection

Plastic filament choices are various and each has different both mechanical and chemical properties; polycarbonate (PC), polyamide (PA) and polyethylene terephthalate-glycol (PETG) plastic filament are chosen for comparison in terms of basic properties, elasticity, etc. as compared in Table IV [25].

TABLE IV
Plastic Filament Comparison

Plastic Properties	PETG	PA	PC
Glass transition temperature (T_g, °C)	73	80–95	113
Modulus of elasticity (GPa)	2.20	0.75	3.24
Ultimate strength (MPa)	53	40–85	72
Density (g $\cdot$ cm^{-3})	1.23	1.06–1.14	1.20
Coefficient of thermal expansion (10^{-6} (°C)$^{-1}$)	60	95	69

Among the choices, firstly, PETG is selected as a main material for major parts and body due to its intermediate elasticity and low shrinkage during printing in FDM 3D printer. Secondly, PC is implemented in battery pack body for its high yield strength as the elasticity of this component is not required. Thirdly, PA is used for elevons due to its high elasticity/flexibility.

C. Delta Wing Designs

The delta wing has a unique attribute being stiffer than other wing shape due to its fully maximized root chord down to zero

tip chord; accordingly, the area of the wing is maximized for the components to fit. Although a rectangular wing has more area, a delta wing is advantageous in terms of aerodynamic efficiency and of being more versatile and efficient in every flight regime: subsonic, transonic and supersonic.

The finalized model design, which is 3D-printed, is separated into three sections for each side to be able to fit in a cylindrical container by folding it on those hinges. The folding mechanism (which each side of the wing is folded three times) and its overall elements are shown in Fig. 8. Spring-integrated hinge is selected being less turbulent between airfoil partitions; additionally, small servo-controlled rod locks those unfolded wings in place after fully deployed from CanSat container.

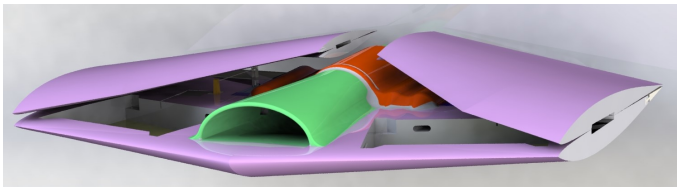

Fig. 8. Folded variant of the delta wing.

The propulsion system is located at the middle of the aircraft, surrounded by electronic components, ESC and a battery pack. The battery pack consists of four Li-ion batteries above which the function of each is stated. The pack connects the system power terminal using XT-60 connectors on both sides of the wing; moreover, it acts as a tightener locking two sides of each wing together to ensure the structural integrity. The design is shown in Fig. 9.

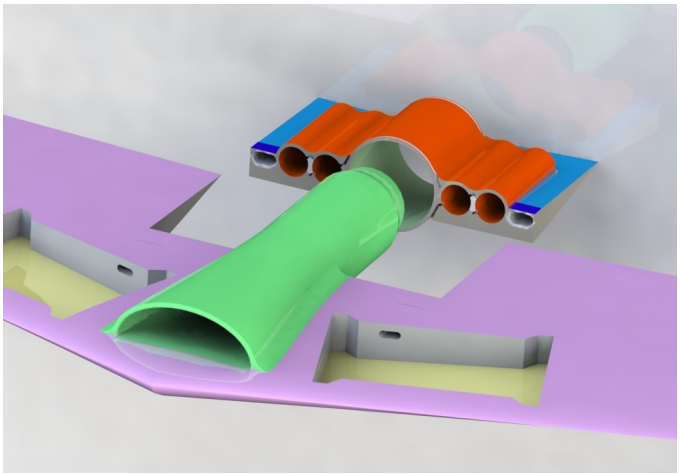

Fig. 9. A battery pack of the delta wing inserting into the main body, which connects two sides together.

Two PCBs are located on both sides of the aircraft, placing parallel to the leading edge of an airfoil, hence more functional area; by locking in place by four bolts on each corner of each PCB, the circuit board and sensors can be disassembled for maintenance with ease.

An elevon, used to control the roll and pitch of an aircraft, has flexible structure which can bend at the fulcrum/joint. It is implemented in an aircraft by creating in a form of an insertion, controlled by a servo on each side, being convenient for replacement in case of malfunctioning or breaking down as shown in Fig. 10.

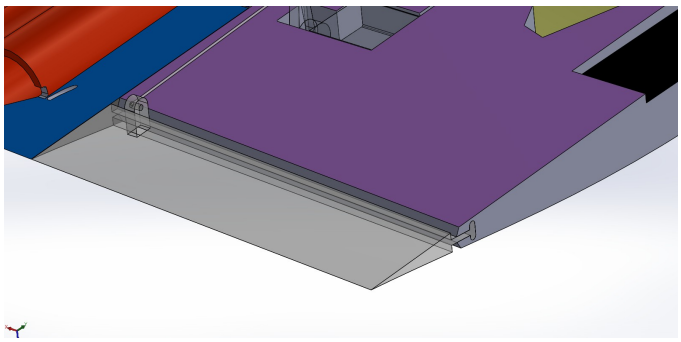

Fig. 10. An elevon on one side.

VI. CanSat Deployment System

A. CanSat Ejection

Needed to be deployed at high altitude, the rocket acts as a carrier which deploys the CanSat at the apogee with single spring release mechanism as elucidated in Fig. 11.

Fig. 11. Single spring release mechanism 3D prototype model.

B. Payload Releasing Mechanism

The releasing mechanism is based on heating nichrome wire to burn the suspension rope within the CanSat container.

VII. Communication and Data Handling Subsystem

A. Data-Related Hardware

The main hardware accountable for data handling subsystem are data controlling hardware and hardware for memory. Classification of hardware by data management are shown in Table V.

TABLE V
DATA HANDLING HARDWARE CLASSIFICATION

Hardware	Communication Type	Usages
Payload Teensy 4.0	Xbee 3 Pro (2.4 GHz)	Transmission of telemetry data parameters to the ground control station
Payload Teensy 4.0	microSD Card Reader Module and microSD Card	Recording sensor data as a backup
Payload Raspberry Pi	microSD Card	Installation of Raspberry Pi OS operating system and video information storage
Container Teensy 4.0	microSD Card Reader Module and microSD Card	Recording sensor data as a backup

B. Communication Protocol

The communication protocol is stratified into two categories: wired communication and wireless communication. Regarding informational conditions and mechanical designs, the usages of both are eventuated in different situations as they are used in CanSat container and the payload (delta wing).

1) Wired Communication: Wired communication is used for transferring data across sensors, modules and microcontrollers. The microSD card reader module with 16 GB microSD card is used for writing string or text information ranging from 64 to 89 bytes per packet long and received from Teensy 4.0 module in comma-delimited format (CSV); moreover, a 32 GB microSD card is chosen for installing Raspberry Pi OS operating system and storing video information in Raspberry Pi Zero W. Additionally, ATMEGA328P is connect to the microSD card reader module which has the same usages as the former. Table VI. entails the protocols for wired communication between telemetry hardware and sensors.

TABLE VI
SENSOR WIRED COMMUNICATION PROTOCOLS

Hardware	Communication Protocol	Usages
ATGM336H	UART	Determination of payload coordinates
BME280	I^2C	Measurement of temperature and air pressure
BNO055	I^2C	Inertial Adjustment
PMS7003	UART	Measurement of air particulates
MPXV7002DP	Analog Voltage	Measurement of differential pressure (airspeed)
microSD Card Reader Module and micro SD Card	SPI	Rewrite-able memory for Teensy 4.0 and Raspberry Pi Zero W

2) Wireless Communication: Wireless communication is used for transmitting the string data to the ground control station in CSV format with downlink frequency of 2.4 GHz. Zigbee Xbee 3 Pro module with omnidirectional monopole antenna is used to serve the purpose. The transmission signal mode is set by XCTU software which modifies NETID/PANID, defines the communication channel and sets the UNICAST transmission mode.

Data on the microSD card is used as a backup to prevent any expected data loss during transmission and to validate the parity of data from wireless communication as the latter is only used for showing real-time data and track the payload on a mission.

C. Telemetry Format

The telemetry is received by the ground station in CSV format. The data is transmitted in 1.0 s time interval between each packet. The sequence, format and byte length of data are shown in Table VII. As regulated and being required for every

TABLE VII
TELEMETRY FORMAT

No.	Parameters	String Size in Bytes	Description
1.	TEAM ID	4	Team identification number assignment
2.	MISSION TIME	1–4	Time in [s] since initial power-up
3.	PACKET COUNT	1–4	Number of transmitted telemetry packets
4.	ALTITUDE	3–6	Altitude relative to ground in [m] with ± 0.01 m resolution
5.	PRESSURE	6–7	Atmospheric Pressure in $[N \cdot m^{-2}]$ or [Pa]
6.	TEMP	4	Temperature in [°C]
7.	VOLTAGE	4	Payload/Container Battery Voltage in [V]
8.	GPS TIME	8	Timestamp generated by GPS T[hh][mm][ss] based on ISO 8601
9.	GPS LATITUDE	9–10	GPS Latitude in [decimal degree]
10.	GPS LONGITUDE	9–10	GPS Longitude in [decimal degree]
11.	GPS ALTITUDE	3–6	GPS Sea-level altitude in [m]
12.	GPS SATS	1–2	Number of satellites tracked by GPS receiver
13.	AIRSPEED	4–5	Speed of payload relative to air in $[m \cdot s^{-1}]$
14.	SOFTWARE STATE	1	Operating software state in one digit number
15.	PARTICLE COUNT	4–6	Air particulates density in $[mg \cdot m^{-3}]$
16.	PITCH	1–4	Pitch angle of the payload relative to Euclidean space (Y-Axis) in [degree]
17.	ROLL	1–4	Roll angle of the payload relative to Euclidean space (X-Axis) in [degree]
18.	YAW AZIMUTH	1–4	Roll or azimuth angle of the payload relative to Euclidean space (Z-Axis) in [degree]

aviation devices, a flight log (inertial data from IMU) and data log are recorded at 40 Hz frequency in a microSD card for further studies and analyses of information.

D. CanSat Antenna Selection

Whereas the 2.4 GHz frequency is used for wireless communication between CanSat and ground control station, 4 dBi IPX connector omnidirectional antenna is selected for transmitting such radio signal; therewith, the mission utilizes frequent changes in heading direction.

VIII. Flight Controlling Software

A. Guidance Method

Consisting of latitude and longitude, a set of GNSS coordinates which creates a closed loop of path is initially actuated and set to create the algorithm which calculates the optimal path that can cover the outside loop. The coordinates of that may be inside the planar loop or along the path of the planar loop. Being comparable to the Convex Hull problem, the task has a number of algorithms to fulfill the requirements of task based on time complexity of possible operations performed by the algorithm. The time complexity is calculated and compared from input size and is defined as a function $O(n)$, $O(n\log n)$, $O(n^{\alpha})$ and other similar forms which n is defined as number of coordinates. Gift Wrapping Algorithm is one of the algorithms in computational geometry which computes the convex hull of a given set of points or coordinates; nonetheless, it does not have the most time complexity efficiency and performance. The worst case time complexity of the gift wrapping algorithm is

$$O(n^2).$$

Conversely, Graham Scan has the worst-case time complexity of

$$O(n\log n).$$

It provides more efficiency of identifying random vertices which extrema may occur. The Graham's Algorithm steps are shown below.

1) Choosing a point O: The origin point O is chosen by either selecting the lowest point of coordinates in Cartesian XY Plane to make the X Axis or selecting the random three points and let O be the centroid of the triangle such that the three points must not be collinear; therefore, let O be the origin point of polar coordinates (r,θ). Being more versatile and efficient, the former is the selected method.

2) Sorting the coordinates: The sorting is done using a lexicographic sort regarding the angle θ from X Axis to $\overline{OP_i}$ with the slope defined as

$$\theta = \begin{cases} \xi & ; \quad \xi > 0 \\ 180^\circ - \xi & ; \quad \xi < 0 \end{cases} \tag{4}$$

while

$$\xi = \arctan\left(\frac{P_i(Y) - O(Y)}{P_i(X) - O(X)}\right) \tag{5}$$

and P_i is an arbitrary point selected by the algorithm.

3) Graham scan method: The Graham scan of the polygon is applied by comparing sets of pair of points (given that the last point is connected with the first point) [24]. The scan starts at the selected lowest point as an extremum and selects the first sorted coordinate (least angle θ). The algorithm aims to eliminate all reflection or reflex vertices by taking three consecutive coordinates and checking whether of those provide a left or right turn relative to O by computing the determinants as stated in (7). Defining matrix

$$\mathbf{A} = \begin{bmatrix} a_x & a_y & 1 \\ b_x & b_y & 1 \\ c_x & c_y & 1 \end{bmatrix} \tag{6}$$

while (a_x,a_y), (b_x,b_y) and (c_x,c_y) are the first, second and third coordinate respectively. The determinant of $\mathbf{A}$ is separated into counterclockwise (CCW), collinear (COL) and clockwise (CW) cases such that

$$\text{CASE} = \begin{cases} \text{CCW} & ; \quad \det(\mathbf{A}) > 0 \\ \text{COL} & ; \quad \det(\mathbf{A}) = 0\,. \\ \text{CW} & ; \quad \det(\mathbf{A}) < 0 \end{cases} \tag{7}$$

Subsequently, the middle vertex (b_x,b_y) is retained provided that the turn is left turn and defined as a tentative convex hull vertex. In case of right turn, the middle vertex is eliminated and reverse the algorithm to check the points $(b_{x,n},b_{y,n})$ whether they are tentative vertices as $n>1$ (origin point is defined as $O(x_1,y_1)$) until it reaches the last point.

4) Convex hull coordinates selection: As the set of coordinates are selected as a closed loop path (a convex hull), it is, accordingly, used by flight direction adjustment algorithm for a delta wing to move along the path. An example of coordinate selection is shown in Fig. 12.

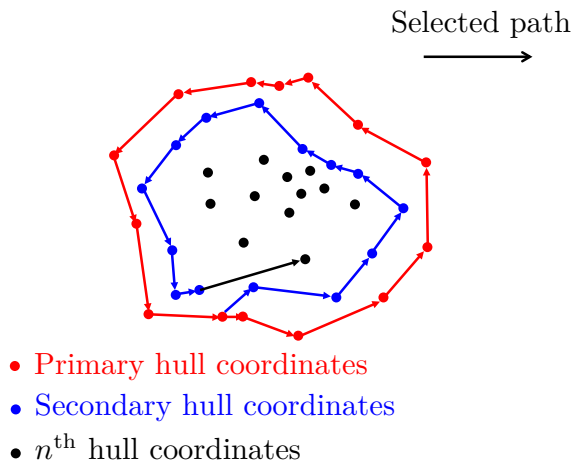

Fig. 12. An example of convex hull (Red = primary hull coordinates, Blue = secondary hull coordinates, Black = n^{th}, arrow = counterclockwise continuous enclosed path).

5) Continuous convex hull: After a primary hull or $(n-1)^{\text{th}}$ hull coordinates are selected and effectuate, a secondary, tertiary, ..., n^{th} hull are selected for a continuous path, joined

at the last point of $(n-1)^{\text{th}}$ set of coordinates and the first point of n^{th} set of coordinates. Until it reaches the last hull, restricted by impossibility of turning (or minimum distance possible), the process will terminate and the aircraft will change the method of descending to Ringsail parachute; consequently a touchdown confirmation will be performed.

B. Flight Direction Adjustment Algorithm

The flight direction has two parts cooperating with each other: guidance direction adjustment and payload self-adjustment. A 3-DOF PID controller algorithm is implemented for adjusting each factor to its designated optimal value; it is already analyzed in MATLAB-Simulink simulation software on dependency of factors, e.g. Moment of Inertia [9], [18], [17].

1) Guidance direction adjustment: There are three different possibilities of flight direction to adjust to: left (LEFT), right (RIGHT) and forward (FWD). Possibilities of those are acquired by calculating the azimuth angle between any two sorted consecutive (X_A, Y_A) and (X_B, Y_B) using equation:

$$\beta = \arctan\left(\frac{X}{Y}\right) \tag{8}$$

while

$$X = \cos(\phi_B) \cdot \sin(\Delta\lambda) \tag{9}$$

and

$$Y = \cos(\phi_A) \cdot \sin(\phi_B) - \sin(\phi_A) \cdot \cos(\phi_B) \cdot \cos(\Delta\lambda) \tag{10}$$

given that

- ϕ_A = Latitude of A;
- ϕ_B = Latitude of B;
- λ_A = Longitude of A;
- λ_B = Longitude of B;
- $\Delta\lambda$ = $\lambda_B - \lambda_A$.

For the LEFT condition, the delta wing needs to adjust its roll to achieve -10° to -15° to get the negative yaw angle; contrarily, +10° to +15° for RIGHT condition to get the positive yaw angle. On the last condition, FWD, the payload needs to stabilize itself to 0° yaw angle. Besides, the pitch angle stays from 5° to 10° to maintain an optimal angle of attack.

2) Payload self-adjustment: The payload needs to calculate its roll to adjust the elevons for effectuating the proper rotational moment for certain case and condition. To prevent any over-rotation, the roll angle of the delta wing is constricted to -20° to 20° range. In case of over-rotation, it will apply moment by controlling the elevons to opposite direction for the adjustments.

C. Aerial Photography

A fixed fish-eye camera is implemented to record the video of the ground during mission; however there are portions of frames which need to be de-stretched out to create true-scale images. OpenCV-Python library can be installed and utilized on Raspberry Pi Zero W with ease.

The camera calibration is required before the usage of undistorting the video, consisting of parameters K and D. The parameters of those can be obtained by printing the checkerboard pattern and capturing the checkerboard pattern in different positions. The function `cv2.cvtColor()` which can convert Blue-Green-Red (BGR) image to grayscale image which can improve the efficiency when using function `cv2.findChessboardCorners()` which can detects corners of the chessboard. Thus, the parameters can be calculated using the function `cv2.fisheye.calibrate()`. Moreover, the functions `cv2.fisheye.initUndistortRectifyMap()` and `cv.remap()` to undistort the video frames by frames. On the mission, the pre-calibration is not required as it is already calibrated and only need to undistort the video.

D. Software State

The software state is a 1 digit number which is a part of the telemetry parameters and reports the current state of operations:

- 0 = Not launched (Rest);
- 1 = Launched but not deployed;
- 2 = Deployed but not landed;
- 3 = Landed;
- 4 = Reset State.

As a result, the delta wing software can reset itself and continue the operations from determination of software state.

IX. Suitability Score Derivation, Calculation and Analysis

Suitability Score is a numerical value indicating a loction's overall suitability for a given land use when all of the suitability factors are considered [27].

The Beta Distribution curve is a probability density function (PDF) used to derive the equation for calculating the suitability value S_β for each term of factor affecting it, for example, atmospheric temperature, humidity, ultraviolet light intensity, electromagnetic radiation within the study area. The suitability value S_β is a function based on parameters, denoted as $S(m, M, t_0, t, \sigma)$; the equation's derivation is detailed as follows. The linear equation:

$$T(t) = at + b \tag{11}$$

is determined as to subside the variable maximum y value of general Beta Distribution equation and to allow such function to vary on x axis. The domain and scale of the function is determined by substituting the function into $T(\frac{t}{M-m})$ and $\frac{m}{m-M}$ into b which produces:

$$X(t) = \frac{t-m}{M-m}\,; \tag{12}$$

such can variate the x-intercept where

- t = measured value;
- m = minimum value on range;
- M = maximum value on range.

The constraints of suitability S_{beta} is determined by substituting the function $X(t)$ into Beta Distribution $B(x)$:

$$B(\xi) = \frac{1}{\left[\frac{\Gamma(\alpha)\Gamma(\beta)}{\Gamma(\alpha+\beta)}\right]} \xi^{\alpha-1}(1-\xi)^{\beta-1} \tag{13}$$

on condition that

$$\begin{aligned} \lim_{\xi\to-\infty} B(\xi) &= \lim_{X(t)\to m^{+}} B(X(t)) \\ &= 0 \end{aligned} \tag{14}$$

and

$$\begin{aligned} \lim_{\xi\to+\infty} B(\xi) &= \lim_{X(t)\to M^{-}} B(X(t)) \\ &= 0 \end{aligned} \tag{15}$$

while $\alpha > 1$ and $\beta > 1$ are arbitrary constants controlling skewness and excess kurtosis in Beta Distribution equation and

$$\begin{aligned} \Gamma(\xi) &= (\xi-1)! \\ &= \int_0^{\infty} e^{-t} t^{\xi-1} \mathrm{d}t. \end{aligned} \tag{16}$$

To compensate the variable maximum value characteristic of Beta Distribution equation, $B(\xi)$ is wholly multiplied by the inverse of maximum value ξ_0 which the value of $B(\xi_0)$ is the maximum, defined by:

$$\xi_0 = \frac{\alpha-1}{\alpha+\beta-2} \quad ; \quad \frac{\mathrm{d}B(\xi)}{\mathrm{d}\xi} = 0. \tag{17}$$

The equation is then derived into:

$$\begin{aligned} B(\xi) &= \frac{1}{B(\xi_0)} \frac{1}{\left[\frac{\Gamma(\alpha)\Gamma(\beta)}{\Gamma(\alpha+\beta)}\right]} \xi^{\alpha-1}(1-\xi)^{\beta-1} \\ B(\xi) &= \frac{\xi^{\alpha-1}(1-\xi)^{\beta-1}}{\xi_0^{\alpha-1}(1-\xi_0)^{\beta-1}} \end{aligned} \tag{18}$$

and

$$S_{\beta} = \frac{(\alpha+\beta-2)\uparrow^2 2}{[(\alpha-1)\uparrow^2 2]\,[(\beta-1)\uparrow^2 2]} (X(t))^{\alpha-1}(1-X(t))^{\beta-1}. \tag{19}$$

By giving $S_{\beta} = 1$ at $t = t_0$, α can be solved as following,

$$\begin{aligned} \frac{\alpha-1}{\alpha+\beta-2} &= \frac{t_0-m}{M-m} \\ \alpha &= \frac{(t_0-m)(\beta-2)+(M-m)}{M-t_0} \end{aligned} \tag{20}$$

and β is based on an arbitrary constant s based on normal distribution fixed parameters:

$$\beta = \frac{1}{\sqrt{2\pi\sigma}} s. \tag{21}$$

As a result, ranging from 0 to 1 or 0% to 100% , the suitability score can be implemented in calculating each impacting factors on human, plants and other living things as needed and find the most suitable area regarding those factors.

X. Ground Control System

The ground control station is utilized to receive string packets from telemetry in CSV format; the data and format is elaborated in Table VII. The system converts CSV string to 1D array which can later be used to display and analyze each term. The operations and designs are categorized into two parts: Software Interface and Hardware as follows.

A. Ground Control Station Hardware and Antenna

Zigbee XBee 3 Pro Module, negotiated by USB Serial Communication, is connected to a portable computer running LabVIEW and Google Earth Pro software to receive 2.4-GHz-wireless signal from the science payload. Attached to Xbee 3 Pro Module with SubMiniature version A (SMA) connector, 2.4 GHz 15 dBi omnidirectional monopole antenna is selected for reasons that the science payload does not need to be tracked in the same manner as a directional antenna. The polar pattern of an omnidirectional antenna is illustrated in Fig. 13

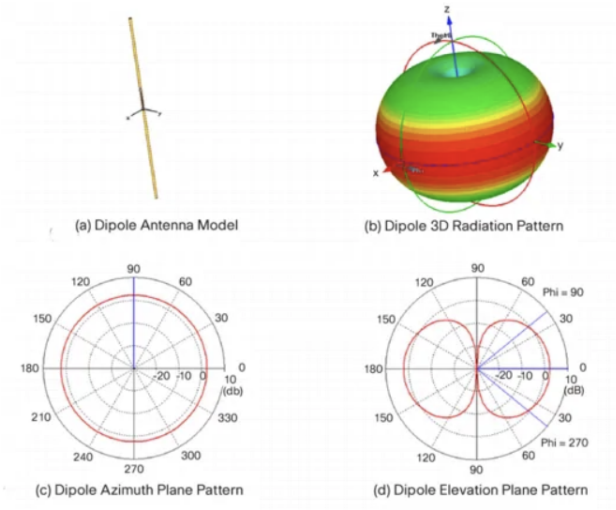

Fig. 13. Polar patterns of a dipole antenna [4].

B. Ground Control Station Software Interface

The software interface of the ground control station is based on LabVIEW software which utilize both front-end interface and back-end system for filtering data, separating columns and rows to 2D array and plot each parameter in a graph. Moreover, Google Earth Pro contributes to LabVIEW in order to plot the coordinates `POS(LAT,LON,ALT)` in 3D illustration with path. The interfaces of the ground control station software are show in Fig. 14. and 15.

1) Receiving data: LabVIEW is installed on a portable computer operating system which is connected to Arduino by means of USB Serial Communication with baud rate of 9600. The software is, then, receive the data from it in CSV string.

2) Filtering data: The software filters data by counting the total number of parameters and checking the range of parameters whether they are in range of possible data. Whole packets are selected on condition that all parameters are complete and healthy. Other packets are eliminated from further processes.

Fig. 14. LabVIEW interface for ground control station.

3) Parameters usages: The parameters are, subsequently, used to display 2D real-time plots of crucial parameters: temperature, altitude, pressure, humidity, airspeed and voltage. The 3D model is also plotted to illustrate the orientation of the model. Furthermore, the numerical parameters in the array are exported to `data-1440.csv` file name by appending with `a+` attributes (appends and updates).

4) Plotting coordinates: LabVIEW has a node to write the sets of coordinates `POS` to two Keyhole Markup Language (KML) files:

1) `gearthlive.kml` for calling and refreshing `gearthcoord.kml` in Google Earth Pro.
2) `gearthcoord.kml` for storing sets of coordinates.

In addition to two mentioned files cooperating with Google Earth Pro, the software periodically imports the coordinates from the KML files and plot them in real time, for instance, the path in Fig. 15. shows a set of lines of height and connecting lines between coordinates.

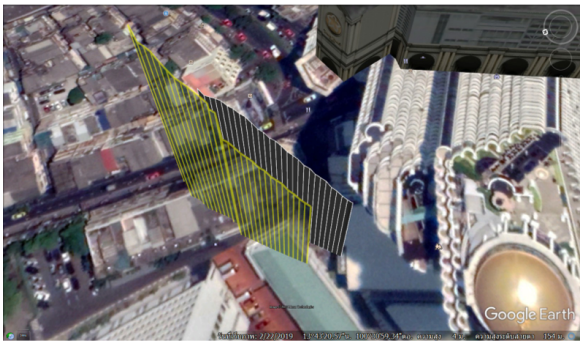

Fig. 15. Google Earth Pro coordinates example plot.

Being advantageous, the real-time plot is used to track the CanSat and recover it on the end of the mission; additionally, the 3D plot can be used to analyze errors, verify area coverage and examine overview of the mission.

XI. Analysis

A. Theoretical Aerodynamic Analysis with Computer Simulation

A 3D Model mesh is fabricated by Autodesk Fusion 360 in Standard Tessellation Language (STL) format which is extensively used in stereolithography field and in Computational Fluid Dynamics software. In addition, global meshes are generated using CFD software which analyzes vortex generation, stall angle, turbulence flow, lift force and drag force of the delta wing.

B. Subsystem Tests

Every different subsystem is assessed of its functionality, efficiency, performance and reliability with distinct methodology. The methods for ensuring that all systems will work with lowest risk possible are applied and described as what follows.

1) Evaluating the functionality of sensors and components, each subsystem is individually tested by inspecting all reported values from Arduino serial monitor.
2) The calculation accuracy and precision of double float variables on Teensy 4.0 are also required to be compared with double float precision on high-precision-and-accuracy computer as the azimuth angle has to be exact to reduce margin of errors.
3) The power consumption and battery usage time is measured and compared with theoretical effectiveness of the power management system and batteries.
4) Wireless communication test is done by placing the CanSat and the ground control station in two positions in different distances while maintaining the line of sight.
5) Temperature test is conducted by placing the CanSat in a temperature test chamber ranging from 25°C to 60°C . The full functionality is examined whether it can operate consistently.

XII. Applications of Aircraft

The delta-wing-based CanSat model can be applied in variety of missions, a strong example of which is to measure and record atmospheric conditions: temperature, humidity, etc. which are to be assessed with numerical and quantitative analysis to determine the survivability of living things or suitability of the study area for the plant to be grown, especially for crops; namely, the suitability equations are described in

Conclusion

This study attempts to create and utilize a delta wing CanSat model, navigation system model, a calculation model and ground control system with simulation and experimental methods. Such models can be utilized in many ways based on the missions and tasks involving the algorithms as elaborated. An integration of subsystems: electronic and power subsystem, descent control methods, mechanical subsystem, deployment, communication and data handling, flight controlling and mathematical analysis are also stated in this paper, being a fully functional system which can be practically operational in a real world condition/situation. Also, quantitative and qualitative approaches are prepared for subsystem integration analysis and data analysis for further actions and usages. Thereafter, a set of experiments in real world is to be done to test the operations

of integrated system, initiated and deployed at a considerable altitude above ground and subsequently analyze the recorded parameters.

Acknowledgment

The authors thank all of the people and organizations who supported their CanSat competition participation, funds for making ALPACA delta-wing CanSat model, MATLAB and LabVIEW software licenses. They also appreciate Bro. Sakda Sakontawat, Ph.D, Bro. Wittaya Thepkomand Nattee Jareankietborworn for supporting funds. They especially appreciate Sunthorn Cloth Store Limited for supporting parachute supply. Moreover, Chulalongkorn University mainly supports analysis tools and equipment for the authors. This work is also supported by faculty of Engineering, King Mongkuts Institute of Technology Ladkrabang. Finally, the authors thank the CanSat Competition 2020 organizers from United States of America and contributors who manage and host the competition.

References

[1] A. Aggarwal, L. J. Guibas, J. Saxe and P. Shor, "A linear time algorithm for computing the Voronoi diagram of a convex polygon," *Proc. 19th Ann. ACM Sympos. Theory Comput.*, pp. 39–45, 1987.

[2] A. Aggarwal, M. M. Klawe, S. Moran, P. Shor and R. Wilber, "Geometric applications of a matrix sorting algorithm," *Proc. 2nd Ann. Sympos. Comput. Geom.*, pp. 285–292, 1986.

[3] B. Chazelle, H. Edelsbrunner and L. J. Guibas, "The complexity of cutting convex polytopes," *Proc. 19th Ann. ACM Sympos. Theory Comput.*, pp. 66–67, 1987.

[4] C. A. Balanis, *Antenna Theory: Analysis and Design*, 4th ed., Hoboken, NJ, USA: John Wiley & Sons, Inc., 2016.

[5] C. Böhm and H. Kriegel, "Determining the Convex Hull in Large Multidimensional Databases," *Data Warehousing and Knowledge Discovery, Third International Conference*, pp. 294–295, 2001.

[6] Cisco, *Dipole Antenna with 3D Radiation Pattern, Azimuth Plane Pattern and Elevation Plane Pattern*. [Online]. Available: https://www.cisco.com/c/en/us/products/collateral/wireless/aironet-antennas-accessories/prod_white_paper0900aecd806a1a3e.html, Accessed on: Sep. 10, 2020.

[7] D. E. Knuth, *Sorting and Searching – the Art of Computer Programming III*. Boston, MA, USA: Addison-Wesley, 1973.

[8] D. G. Kirkpatrick and R. Seidel, "The ultimate convex hull algorithm?," *SIAM J. Comput.*, vol. 15, pp. 287–299, 1986.

[9] D. G. Kirkpatrick and R. Seidel, "Design and Tuning Approach of 3-DOF Emotion Intelligent PID (3-DOF-PID) Controller," *2012 Sixth UKSim/AMSS European Symposium on Computer Modeling and Simulation*, pp. 74–77, 2012. DOI: 10.1109/EMS.2012.93, [Online].

[10] E. G. Ewing, *RINGSAIL PARACHUTE DESIGN*. Springfield, VA, USA: National Technical Information Service, 1972, pp. 24–58.

[11] Ema Design Automation, *The Hitchhiker's Guide to PCB Design*. San Francisco, CA, USA: Blurb, 2019, pp. 25–78.

[12] F. P. Preparata and M. I. Shamos, *Computational Geometry – an Introduction*. New York, NY, USA: Springer-Verlag, 1985.

[13] G. L. Faurote, *DESIGN OF DISK-GAP-BAND AND MODIFIED RINGSAIL PARACHUTES AND DEVELOPMENT OF BALLUTE APEX INLET FOR SUPERSONIC APPLICATION*. Akron, OH, USA: GOODYEAR AEROSPACE CORPORATION, 1970, pp. 1–32.

[14] I. D. Faux and M. J. Pratt, *Computational Geometry for Design and Manufacture*. Hoboken, NJ, USA: John Wiley & Sons, 1981.

[15] J. D. Kraus and R. J. Marthefka, *Antennas for all applications*. New York City, NY, USA: McGraw-Hill, 2002.

[16] J. K. Parker, *An Introduction to High-Altitude Space Use of GNSS (For Timing People)*. [Online]. Available: https://www.gps.gov/cgsic/meetings/2018/parker.pdf, Accessed on: Sep. 14, 2020.

[17] K. H. Ang and G. Chong, "PID Control System Analysis, Design, and Technology," *IEEE Transactions on Control Systems Technology*, vol. 13, no.4, pp. 559–576, Aug. 2005.

[18] K. J. Astrom and R. M. Murray, *Feedback Systems: an Introduction for Scientists and Engineers*. 2nd ed., Priceton, NJ, USA: Priceton Univ. Press, 2008.

[19] K. Mehlhorn, *Multidimensional Searching and Computational Geometry*. Heidelberg, Germany: Springer-Heidelberg, 1984.

[20] M. Blurb, R. W. Floyd, V. R. Pratt, R. L. Rivest and R. E. Tarjan, "Time bounds for selection," *J. Comput. System Sci.*, vol. 7, pp. 448–461, 1972.

[21] M. I. Minski and S. Papert, *Perceptrons, An Introduction to Computational Geometry*. Cambridge, MA, USA: MIT Press, 1969.

[22] M. S. Selig, J. J. Guglielmo, A. P. Broeren and and P. Giguère, *Summary of Low-Speed Airfoil Data*, vol. 1, 1995, pp. 33–34.

[23] P. R. Delurgio, "EVOLUTION OF THE RINGSAIL PARACHUTE," *CEAS/AIAA Aerodynamic Decelerator Systems Technology Conference*, pp. 1–10, June. 1999. DOI: 10.2514/6.1999-1700, [Online].

[24] P. T. An, "A modification of Graham's algorithm for determining the convex hull of a finite planar set," *Annales Mathematicae et Informaticae*, vol. 35, pp. 3–8, Oct. 2007.

[25] V. D. Sagias, K. I. Giannakopoulos, C. Stergiou, "Mechanical properties of 3D printed polymer specimens," *Procedia Structural Integrity*, pp. 85–90, Jan. 2018. DOI: 10.1016/j.prostr.2018.09.013, [Online].

[26] W. E. Souder, "A Scoring Methodology for Assessing the Suitability of Management Science Models," *Management Science, Application Series*, vol. 18, no.10, pp. B526–B543, Jun. 1972.

[27] What if?, *7: Analyzing Suitability*. [Online]. Available: http://whatifinc.biz/im/docs/Analyzing_Suitability.pdf, Accessed on: Sep. 26, 2020.